Cramér-Rao bounds for attitude estimation using signals with unknown structure

Lubbers, Barend; Heusdens, Richard

DOI
10.1109/TVT.2025.3574770

Publication date
2025

Document Version
Final published version

Published in
IEEE Transactions on Vehicular Technology

Cramér–Rao Bounds for Attitude Estimation Using Signals With Unknown Structure

Barend Lubbers and Richard Heusdens, *Senior Member, IEEE*

***Abstract*—Direction-of-arrival (DOA) estimation can be used for many different applications. In this paper the classical DOA estimation is modified to estimate the attitude of an antenna array when the DOAs of sources are given. Usually DOA attitude estimation assumes knowledge on the structure of the used signals. In this paper signals with an unknown structure are used for attitude estimation. The theoretical best performance is determined by deriving the Cramér-Rao lower bounds for attitude estimation based on two different signal models: the deterministic and stochastic signal model. Next, the attitude estimation performance of both signal models are compared to each other. It is shown that for high signal-to-noise ratios (SNRs) both models perform equally well. If the SNR drops, both models perform equally if the number of sources is low with respect to the number of antenna elements. For a large number of sources, the stochastic model outperforms the deterministic model unless the SNR drops too low. For very low SNRs, the deterministic outperforms the stochastic model regardless of the number of sources.**

***Index Terms*—Antenna arrays, radio navigation, satellite navigation systems.**

I. Introduction

DIRECTION-OF-ARRIVAL (DOA) estimation of radio signals using antenna arrays is used in many applications such as radar, sonar and communication networks [1], [2]. Conversely, if the DOAs of radio sources are known beforehand, these DOAs can be used to provide attitude information of the antenna array [3], [4], [5]. This antenna attitude can provide attitude information of a platform such as a vehicle, ship or aircraft.

Information about the attitude of a platform, e.g. pitch, roll and/or heading, is important information for navigation, (flight) control and many other applications. This information is usually obtained by a combination of sensors, for example (optical) gyroscopes, accelerometers, (gyro)compasses and/or magnetometers [6]. A fundamentally different method of attitude determination is by using radio signals, such as the signals transmitted by satellites. In particular global navigation satellite system (GNSS) signals, such as those of the global positioning system (GPS) are well suited for this application [7], [8], [9].

There are basically two methods for attitude estimation using GNSS signals. The first and most commonly used method depends on the relative positioning of two antennas with respect to a common reference antenna, all placed on a single platform. The relative positioning of the antennas is based on the carrier phase observations. GNSS carrier phase observations are very precise, however, they are ambiguous. To obtain precise attitude information, these ambiguities have to be solved. For this the (multivariate constrained) least-squares ambiguity decorrelation adjustment (LAMBDA) [10] method is often used [9], [11]. An in depth overview of GNSS carrier phase based attitude estimation is given in [12] and [13].

The second method for GNSS attitude estimation is based on DOA estimation techniques [4], [14], [15]. If the azimuth and elevation of two or more sources are known with respect to the local horizontal plane, e.g. in an north-east-down (NED) or east-north-up (ENU) reference frame, the DOAs of the signals can be used to determine the rotations or attitude of the antenna with respect to the local horizontal plane reference frame [16]. It is important to realise that this is fundamentally different than classical DOA estimation, although it might look similar at first sight. The fundamental difference between classical DOA estimation and the presented attitude estimation is in the unknown parameters. In classical DOA estimation the individual angles of arrival are the unknown parameters of interest. It is assumed that the attitude of the antenna is known and hence the direction of the signals can be determined. The proposed method of attitude estimation is the inverse problem; the angles of arrival are assumed to be known while the attitude of the antenna is unknown. The attitude of the antenna can be expressed by three (Euler) angles; roll, pitch and yaw. In attitude estimation there are, therefore, always three unknown parameters of interest, regardless of the number of signals used. For classical DOA estimation there are for each signal two unknown parameters of interest (azimuth and elevation), so in total twice the number of signals.

An efficient implementation of this DOA based attitude estimation method is described in detail in [3]. Many implementations, like the one described in [15], first estimate the DOAs of each source with respect to the antenna separately, after which the attitude of the array is determined based on the known azimuth en elevation of the individual sources in the local horizontal plane reference frame. There is, however,

Received 24 July 2024; revised 12 November 2024 and 28 April 2025; accepted 13 May 2025. Date of publication 6 June 2025; date of current version 20 November 2025. The review of this article was coordinated by Prof. Zhiguo Shi. *(Corresponding author: Barend Lubbers.)*

Barend Lubbers is with the Netherlands Defence Academy (NLDA), Faculty of Military Sciences 1781 AC Den Helder, The Netherlands (e-mail: b.lubbers.02@mindef.nl).

Richard Heusdens is with the Netherlands Defence Academy (NLDA), Faculty of Military Sciences 1781 AC Den Helder, The Netherlands, and also with the Faculty of Electrical Engineering, Mathematics and Computer Science, Delft University of Technology, 2628 CD Delft, The Netherlands (e-mail: r.heusdens@mindef.nl,tudelft.nl).

Digital Object Identifier 10.1109/TVT.2025.3574770

a way to determine the antenna attitude directly, without the need of estimating each DOA separately [3], [4], [5]. As the positions (azimuths and elevations) of the sources are known, these can be used as a constraint for the relative positions between the sources. With this constraint, the steering vectors can be calculated a-priori based on the azimuth and elevation of each source in the local horizontal plane frame. Now all the steering vectors as a combination should undergo the same rotations until all steering vectors match the incoming signals. These rotations represent the attitude angles of the antenna. This way the antenna attitude is determined directly, without the need for DOA estimations of the individual signals. This results in only three unknown parameters instead of 3 unknown attitude angles and 2 unknown DOA angles for each source.

Most attitude determination methods, including all methods described above, rely on signals that are in code and/or Doppler/carrier track. For the first method mentioned above this is required as the method relies on the output of the carrier tracking loop of the receivers. For the second method this is not strictly required, although it will drastically increase the signal-to-noise ratio (SNR). With the code removed from the signal, the bandwidth is reduced from 2 MHz (for the C/A code) to 100 Hz. This allows for filtering with a much smaller bandwidth and thus reducing the noise and increasing the SNR. With the Doppler shift known, also the frequency of the remaining carrier signal is known. To be in code and Doppler track, the signal structure, in this case the code and its modulation, needs to be known. These are known for the civil GPS signals, e.g. C/A, L2C, L1C and L5, or other open GNSS signals. However, the encrypted signals such as the GPS P(Y) and M-code or Galileo PRS cannot be used. So, the methods described above cannot be used for signals with unknown structure, which limits its applicability.

In this paper we consider DOA based attitude estimation without using the signal structure. This allows for the use of encrypted GNSS signals, but also for many (encrypted) non-GNSS signals. The use of unknown signals opens huge possibilities with the expanding satellite constellations. Especially the current developments on low-earth orbit position navigation and timing (LEO-PNT) satellite constellations [17], and the massive communications/internet constellations such as Starlink, OneWeb and Project Kuiper (Amazon), consisting of hundreds or even thousands of satellites [18], [19], [20]. We will consider two different models when dealing with unknown signals: the deterministic signal model (DM) and the stochastic signal model (SM). In literature these models are sometimes referred to as the conditional and unconditional signal models, respectively [21], [22]. With the DM no assumptions are made on the signals and at each time instance they are regarded as unknown parameters that have to be estimated. With the SM, the signals are modelled as stationary stochastic processes with a certain probability distribution and an unknown covariance matrix which needs to be estimated. The performance of these DM and SM signal models is studied by calculating the Cramér-Rao lower bounds (CRB). These give the lowest possible variance of the unbiased estimation of unknown parameters, in this case the attitude of the antenna array. The found CRBs for the DM and SM are valid for attitude determination using arbitrary radio signals. The only requirement on the signals is that the transmitters are in the far field and that the location of the transmitters, in terms of azimuth and elevation in an horizontal plane reference frame, is known. Further it is highly desirable that the sources are more or less uniformly distributed around the receiver. Based on these requirements GNSS signals are perfectly suited, but other satellite systems or combinations of systems might even be better candidates. Especially the new LEO navigation and communication constellations, as mentioned before, could be perfect candidates due to the extremely dense constellation of thousands of satellites. Terrestrial sources are less suited as these are mostly located near the horizon and hence are more or less located in a single plane. Every known aspect of the signals should be exploited and will increase the accuracy. In this paper, however, the CRB is determined for the worst case where nothing of the signals is known.

In this paper the CRB for the DM is derived and compared with the CRB of the SM. The evaluated bounds are a measure for the best possible performance of the attitude estimation based on both models. The CRBs are independent of actual algorithms, therefore, in this paper no algorithm is provided to estimate the attitude. The CRBs are determined for three main reasons. The first reason is to allow us to determine the validity of antenna array based attitude estimation using unknown signals. It allows us to determine the minimal requirements on antenna size and geometry, number and SNR of the used signals and the measurement length (number of samples) to obtain a certain required performance. The theory in this paper also allows us to compare the expected performance to existing method of attitude estimation. Secondly, to determine which signal model (SM or DM) is best under which conditions. Thirdly, to enable the assessment of algorithms developed in future research.

A. Main Contributions

This paper contains the following main contributions:

- Provide the theory to enable the quantification of the performance of antenna array based attitude estimation using unknown signals.
- Derivation and validation of the CRB of attitude estimation based on the stochastic and deterministic signal models
- Derivation of the CRB of attitude estimation for the stochastic model for the case with low SNR and a large number of antenna elements

B. Organization of the Paper

This paper is organised in the following way. In the next section the observation models for the DM and SM are introduced. In Section IV the CRBs based on the observation models for the DM and SM are provided after which, in Section V, the bounds are compared to each other for different settings of parameters. In Section VI we explain the behaviour of the bounds using a theoretical analysis of the CRB of a simplified two-dimensional case study. In Section VII the found CRBs are compared to estimated variances based on Monte-Carlo simulations of the estimation of the antenna attitude angles. Finally the conclusions are drawn in Section VIII.

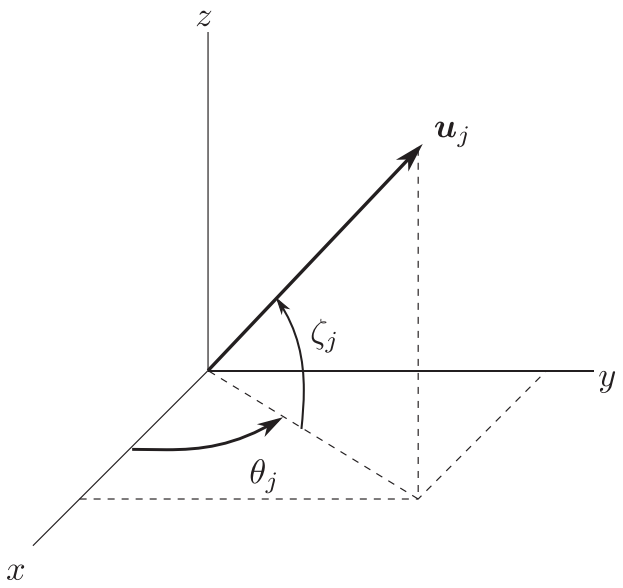

Fig. 1. Definition of azimuth, θ_j, and elevation, ζ_j, angles.

II. Nomenclature

The following notations are used throughout this paper. Scalars are represented by lower case characters. Vectors are represented by bold lower case characters and are by default in column orientation. Matrices are represented by bold upper case characters. $\boldsymbol{I}_m$ denoted the $m \times m$ identity matrix. Matrix transposition is indicated by the superscript T, the conjugate or Hermitian transpose by the superscript H and the conjugate by the superscript $*$. Further $\mathbb{E}(.)$ denotes statistical expectation, $\mathrm{tr}(.)$ denotes the trace, and $|.|$ the determinant operators. Finally, the Kronecker product is denoted by $\otimes$ and the Hadamard (element wise) product by $\odot$.

III. Observation Models

Suppose we receive r signals on an arbitrary antenna array with m elements, where $r < m$. The received signals can then be modelled by

$$\boldsymbol{y}(t) = \boldsymbol{A}(\boldsymbol{\theta}, \boldsymbol{\zeta})\boldsymbol{s}(t) + \boldsymbol{v}(t), \quad t = 1, \ldots, n,$$

where $\boldsymbol{y}(t) \in \mathbb{C}^m$ is the observation vector, $\boldsymbol{A}(\boldsymbol{\theta}, \boldsymbol{\zeta}) \in \mathbb{C}^{m \times r}$ the matrix who's columns are the r steering vectors to each source and $\boldsymbol{\theta}$ and $\boldsymbol{\zeta}$ are vectors containing the azimuth and elevation angles to each transmitter, see Fig. 1 for its definitions. The azimuth and elevation angles are given in a local tangent plane frame [6, p. 28]. Further, $\boldsymbol{s}(t) \in \mathbb{C}^r$ are the received signals and $\boldsymbol{v}(t) \in \mathbb{C}^m$ is the noise vector which is assumed to be zero-mean and circularly-symmetric complex Gaussian, $\boldsymbol{v}(t) \sim \mathcal{CN}(0, \boldsymbol{R}_v)$, where $\boldsymbol{R}_v$ is the $m \times m$ noise covariance matrix.

The matrix with steering vectors is given by

$$\boldsymbol{A}(\boldsymbol{\theta}, \boldsymbol{\zeta}) = [\boldsymbol{a}(\theta_1, \zeta_1), \ldots, \boldsymbol{a}(\theta_r, \zeta_r)],$$

where $\boldsymbol{a}(\theta_j, \zeta_j), j = 1, \ldots, r$, are the individual steering vectors given by

$$\boldsymbol{a}(\theta_j, \zeta_j) = \left[\exp(i\kappa \boldsymbol{b}_1^T \boldsymbol{u}_j), \ldots, \exp(i\kappa \boldsymbol{b}_m^T \boldsymbol{u}_j)\right]^T, \quad (1)$$

where $\kappa = \frac{2\pi}{\lambda}$ is the wave number and λ the wavelength,[1] $\boldsymbol{b}_k \in \mathbb{R}^3$ is the position vector of the kth antenna element, and $\boldsymbol{u}_j \in \mathbb{R}^3$ the line-of-sight vector of source j given by

$$\boldsymbol{u}_j = \begin{bmatrix} \cos(\theta_j)\cos(\zeta_j) \\ \sin(\theta_j)\cos(\zeta_j) \\ \sin(\zeta_j) \end{bmatrix}.$$

Both $\boldsymbol{b}_k$ and $\boldsymbol{u}_j$ are defined in a local tangent plane frame with the axes in the directions of East, North and Up (ENU). The antenna geometry can be defined by a matrix

$$\begin{aligned} \boldsymbol{B} &= [\boldsymbol{b}_1, \ldots, \boldsymbol{b}_m] \\ &= \boldsymbol{C}(\boldsymbol{\gamma})\boldsymbol{G} \\ &= \boldsymbol{C}(\boldsymbol{\gamma})[\boldsymbol{g}_1, \ldots, \boldsymbol{g}_m] \end{aligned}$$

where $\boldsymbol{g}$ is a vector with the x, y and z coordinates of the antenna elements in a local antenna reference frame. $\boldsymbol{C}(\boldsymbol{\gamma})$ is the rotation/transformation matrix from the antenna reference frame to the ENU reference frame by rotations around the x, y and z axis of the antenna frame. The angles of rotation are given by $\boldsymbol{\gamma} = [\gamma_x, \gamma_y, \gamma_z]$ and the rotation matrix is given by

$$\boldsymbol{C}(\boldsymbol{\gamma}) = \boldsymbol{C}_x(\gamma_x)\boldsymbol{C}_y(\gamma_y)\boldsymbol{C}_z(\gamma_z)$$

where

$$\boldsymbol{C}_x(\gamma_x) = \begin{bmatrix} 1 & 0 & 0 \\ 0 & \cos\gamma_x & \sin\gamma_x \\ 0 & -\sin\gamma_x & \cos\gamma_x \end{bmatrix},$$

$$\boldsymbol{C}_y(\gamma_y) = \begin{bmatrix} \cos\gamma_y & 0 & -\sin\gamma_y \\ 0 & 1 & 0 \\ \sin\gamma_y & 0 & \cos\gamma_y \end{bmatrix},$$

$$\boldsymbol{C}_z(\gamma_z) = \begin{bmatrix} \cos\gamma_z & \sin\gamma_z & 0 \\ -\sin\gamma_z & \cos\gamma_z & 0 \\ 0 & 0 & 1 \end{bmatrix}.$$

For notational convenience we will drop the dependency on $\boldsymbol{\gamma}$ and simply write $\boldsymbol{C}$ instead of $\boldsymbol{C}(\boldsymbol{\gamma})$. In addition, it is assumed that $\boldsymbol{\theta}$ and $\boldsymbol{\zeta}$ are known and that the only unknown parameters in the steering vectors are the antenna attitude angels $\boldsymbol{\gamma}$. As $\boldsymbol{\theta}$ and $\boldsymbol{\zeta}$ are considered known, from here on the dependency on $\boldsymbol{\theta}$ and $\boldsymbol{\zeta}$ is omitted and $\boldsymbol{A}(\boldsymbol{\theta}, \boldsymbol{\zeta})$ and $\boldsymbol{a}(\theta_j, \zeta_j)$ are referred to as $\boldsymbol{A}$ and $\boldsymbol{a}_j$ respectively. With this, (1) can be rewritten as

$$\boldsymbol{a}_j = \left[\exp(i\kappa \boldsymbol{g}_1^T C^T \boldsymbol{u}_j), \ldots, \exp(i\kappa \boldsymbol{g}_m^T C^T \boldsymbol{u}_j)\right]^T,$$

where $j = 1, \ldots, r$, which allows us to easily rotate the steering vectors with respect to the antenna reference frame.

Finally, we have to define the models for the signals $\boldsymbol{s}(t)$. In this paper two different models are considered, the deterministic model (DM) and the stochastic model (SM).

A. Deterministic Model

The DM does not make any assumption on the signal, except that the signal is deterministic. As the signals are unknown these have to be estimated for each sample. For the DM, the number of unknown parameters is therefore $4 + 2rn$ in total; 3 rotation

[1] It is assumed that the variations in the frequency, for example due to Doppler shift, are small compared to the carrier frequency.

angles, σ^2 and the real and imaginary part of the r signal samples for all n observations (more on this in the following section).

B. Stochastic Model

The SM assumes that the signals are realizations of stationary stochastic processes. It is common to assume that $\boldsymbol{s}(t)$ is zero-mean circularly-symmetric complex Gaussian distributed [21]

$$\boldsymbol{s}(t) \sim \mathcal{CN}(0, \boldsymbol{R}_s),$$

with covariance matrix $\boldsymbol{R}_s$.

The covariance of the observations $\boldsymbol{y}(t)$ is then given by:

$$\boldsymbol{R} = \boldsymbol{A}\boldsymbol{R}_s\boldsymbol{A}^H + \sigma^2\boldsymbol{I}_m,$$

where we assume that $\boldsymbol{R}_v = \sigma^2\boldsymbol{I}_m$. In this paper it is assumed that the received signals are mutually uncorrelated an therefore the covariance matrix $\boldsymbol{R}_s$ is given by $\boldsymbol{R}_s = \text{diag}(p_1, \ldots, p_r)$, with p_i the received power of source i. Hence, the source signals are statistically independent, but not identically distributed.

Usually the covariance matrix $\boldsymbol{R}_s$ is unknown and needs to be estimated. For the SM model, the number of unknown parameters is therefore $4 + r$ in total; 3 unknown rotation angles, σ^2 and the r diagonal elements of $\boldsymbol{R}_s$. In the case where the signal cannot be assumed uncorrelated, hence the covariance matrix is non-zero on the off-diagonal elements, the total of unknown parameters becomes $4 + r^2$.

IV. Cramér Rao Lower Bound

To study the theoretical best possible performance of the attitude estimation, the Cramér-Rao bound (CRB) is calculated. The CRB gives the lowest possible variance of any unbiased estimator and is defined as the diagonal of the inverse Fisher information matrix (FIM). The elements of the FIM are defined as [23]

$$\{\text{FIM}(\boldsymbol{\xi})\}_{jl} = \mathbb{E}\left[\frac{\partial l(\boldsymbol{\xi};\boldsymbol{Y})}{\partial \boldsymbol{\xi}_j}\frac{\partial l(\boldsymbol{\xi};\boldsymbol{Y})}{\partial \boldsymbol{\xi}_l}\right] = -\mathbb{E}\left[\frac{\partial^2 l(\boldsymbol{\xi};\boldsymbol{Y})}{\partial \boldsymbol{\xi}_j \partial \boldsymbol{\xi}_l}\right],$$

where $l(\boldsymbol{\xi};\boldsymbol{Y})$ is the log-likelihood function, $\boldsymbol{\xi}$ is the vector with unknown parameters to be estimated, and $\boldsymbol{Y} = [\boldsymbol{y}(1), \ldots, \boldsymbol{y}(n)]$. As both signal models have different likelihood functions, the FIM and hence the CRB will be different for each model. In this section the CRBs of the DM and SM are derived, after which, in Section V, they are compared to each other to determine which signal model is potentially more efficient in which scenario.

A. Deterministic Model

The log-likelihood function of the observed data under the DM is given by

$$\begin{aligned} l(\sigma^2, \boldsymbol{S}, \boldsymbol{\gamma}) &= \ln p(\boldsymbol{Y}; \sigma^2, \boldsymbol{S}, \boldsymbol{\gamma}) \\ &= -mn\ln(\pi\sigma^2) \\ &\quad - \frac{1}{\sigma^2}\sum_{t=1}^{n} \|\boldsymbol{y}(t) - \boldsymbol{A}\boldsymbol{s}(t)\|_2^2, \end{aligned} \tag{2}$$

where $\boldsymbol{S} = [\boldsymbol{s}(1), \ldots, \boldsymbol{s}(n)]$. Because the unknown signal $\boldsymbol{s}(t)$ is complex valued, the partial derivatives of the log-likelihood function to $\boldsymbol{s}(t)$ are Wirtinger derivatives [24]. This means that the log-likelihood function must be differentiated with respect to both $\boldsymbol{s}(t)$ and its complex conjugate $\boldsymbol{s}^*(t)$. Hence, we have the following $4 + 2nr$ unknown parameters

$$\begin{aligned} \boldsymbol{\xi} = \big[&\sigma^2, \text{Re}\left(\boldsymbol{s}(1)^T, \ldots, \boldsymbol{s}(n)^T\right), \\ &\text{Im}\left(\boldsymbol{s}(1)^T, \ldots, \boldsymbol{s}(n)^T\right), \boldsymbol{\gamma}\big]^T, \end{aligned}$$

which need to be estimated.

Let $\boldsymbol{1}_r$ denote the length r all ones vector, and $\mathbb{1}_3$ the 3×3 all ones matrix ($\mathbb{1}_3 = \boldsymbol{1}_3 \otimes \boldsymbol{1}_3^T$). Moreover, let $\boldsymbol{P}_{\boldsymbol{A}}^{\perp}$ denote the orthogonal projection operator onto the null space of $\boldsymbol{A}$

$$\boldsymbol{P}_{\boldsymbol{A}}^{\perp} = \boldsymbol{I}_m - \boldsymbol{A}(\boldsymbol{A}^H\boldsymbol{A})^{-1}\boldsymbol{A}^H,$$

and let $\partial_{\boldsymbol{\gamma}}(\boldsymbol{A})$ be defined as

$$\partial_{\boldsymbol{\gamma}}(\boldsymbol{A}) = \left[\partial_{\gamma_x}(\boldsymbol{A}), \partial_{\gamma_y}(\boldsymbol{A}), \partial_{\gamma_z}(\boldsymbol{A})\right],$$

where

$$\begin{aligned} \partial_{\gamma_j}(\boldsymbol{A}) &= \frac{\partial \boldsymbol{A}}{\partial \gamma_j} \\ &= \left[\frac{\partial \boldsymbol{a}_1}{\partial \gamma_j}, \ldots, \frac{\partial \boldsymbol{a}_r}{\partial \gamma_j}\right], \quad j \in \{x, y, z\}. \end{aligned}$$

Finally, let $\boldsymbol{S}_d(t) = \boldsymbol{I}_3 \otimes \boldsymbol{s}(t)$. We have the following result.

Theorem 1: The Cramér-Rao lower bound for estimating $\boldsymbol{\xi}$ is given by

$$\begin{aligned} \text{CRB}_{\text{DM}}(\boldsymbol{\xi}) = \sigma^2 \Bigg[2\sum_{t=1}^{n} \text{Re}\big\{&\boldsymbol{S}_d^H(t)\partial_{\boldsymbol{\gamma}}(\boldsymbol{A})^H \\ &\boldsymbol{P}_{\boldsymbol{A}}^{\perp}\partial_{\boldsymbol{\gamma}}(\boldsymbol{A})\boldsymbol{S}_d(t)\big\}\Bigg]^{-1}. \end{aligned} \tag{3}$$

Proof: See Appendix A. □

Corollary 1: For sufficiently large n, the Cramér-Rao lower bound for estimating $\boldsymbol{\xi}$ is given by

$$\begin{aligned} \text{CRB}_{\text{DM}}(\boldsymbol{\xi}) = \frac{1}{2n}\sigma^2 \Big[\text{Re}\Big\{&(\boldsymbol{I}_3 \otimes \boldsymbol{1}_r)^T \\ &\left\{\partial_{\boldsymbol{\gamma}}(\boldsymbol{A})^H\boldsymbol{P}_{\boldsymbol{A}}^{\perp}\partial_{\boldsymbol{\gamma}}(\boldsymbol{A}) \odot (\mathbb{1}_3 \otimes \boldsymbol{R}_s)\right\}(\boldsymbol{I}_3 \otimes \boldsymbol{1}_r)\Big\}\Big]^{-1}, \end{aligned} \tag{4}$$

Proof: See Appendix B. □

B. Stochastic Model

Under the stochastic model, the log-likelihood function of the observed data is given by

$$\begin{aligned} l(\sigma^2, \boldsymbol{R}_s, \boldsymbol{\gamma}) &= \ln p(\boldsymbol{Y}; \sigma^2, \boldsymbol{R}_s, \boldsymbol{\gamma}) \\ &= -mn\ln\pi - n\ln|\boldsymbol{R}| - \sum_{t=1}^{n}\boldsymbol{y}^H(t)\boldsymbol{R}^{-1}\boldsymbol{y}(t) \\ &= -mn\ln\pi - n\ln|\boldsymbol{R}| - n\text{tr}(\boldsymbol{R}^{-1}\hat{\boldsymbol{R}}), \end{aligned}$$

where

$$\hat{\boldsymbol{R}} = \frac{1}{n}\sum_{t=1}^{n}\boldsymbol{y}(t)\boldsymbol{y}^H(t),$$

the sample covariance matrix. Hence, under the SM, we have the following unknown parameters

$$\boldsymbol{\xi} = \left\{\sigma^2, \boldsymbol{\gamma}, \boldsymbol{R}_s\right\},$$

which, under the assumption of a diagonal $\boldsymbol{R}_s$, reduces to

$$\boldsymbol{\xi} = \left\{\sigma^2, \boldsymbol{\gamma}, p_1, \ldots, p_r\right\}.$$

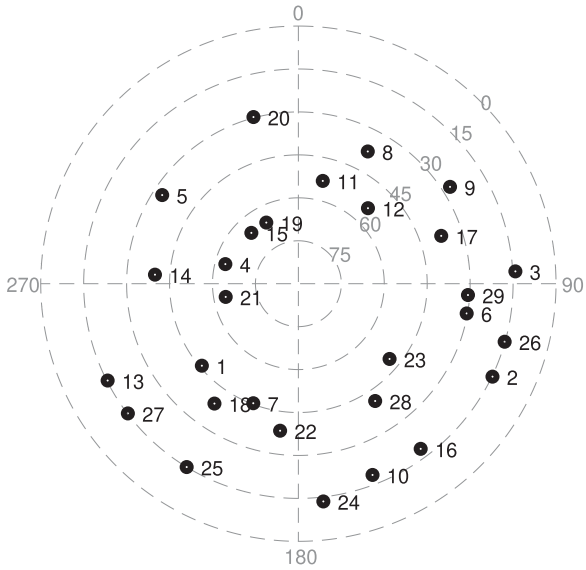

Fig. 2. Geometry of the 29 sources as used for the comparison of the DM and SM.

The elements of the FIM for the SM are given by [22]

$$\{\boldsymbol{F}_{\mathrm{SM}}\}_{jl} = n\,\mathrm{tr}(\boldsymbol{R}^{-1}\partial_{\boldsymbol{\xi}_j}(\boldsymbol{R})\boldsymbol{R}^{-1}\partial_{\boldsymbol{\xi}_l}(\boldsymbol{R}))), \tag{5}$$

where

$$\partial_{\boldsymbol{\xi}_j}(\boldsymbol{R}) = \frac{\partial \boldsymbol{R}}{\partial \xi_j} \quad \text{and} \quad \partial_{\boldsymbol{\xi}_l}(\boldsymbol{R}) = \frac{\partial \boldsymbol{R}}{\partial \xi_l}.$$

With this, the CRB is given by

$$\mathrm{CRB}_{\mathrm{SM}} = \boldsymbol{F}_{\mathrm{SM}}^{-1}, \tag{6}$$

where we are only interested in the elements associated with the variance of the attitude angles $\boldsymbol{\gamma}$. Note that although the equation has the same structure as in [22], the unknown parameters are different, and therefore different derivatives are used in the evaluation of the equation. A closed-form formula for the CRB under the SM is not available. For the comparison of both models this is not strictly required, although it might provide more insight in the properties of the SM and its CRB. In Section VI an expression for the special case with low SNR and large m is provided with Theorem 2.

V. CRB Comparison for the SM and DM

In this section, the CRBs of the SM and the DM are compared for different SNR levels and different number of antennas. Different values for n are not considered because the bound decreases inversely proportional to n, as can be seen from (4) and (6). For all comparisons, the number of samples, n, is therefore fixed at 10^3.

Comparisons are made based on a fixed geometry of the sources, which is given in the sky plot in Fig. 2. The sources are randomly placed and remain fixed for all scenarios. If r sources are used, only the first r sources are considered, where a maximum of 29 sources is used (resulting in a maximum antenna array size of 30 elements). In addition, $\boldsymbol{R}_s$ is fixed for all scenarios. This (diagonal) covariance matrix is constructed by choosing the diagonal elements uniformly at random between 0.75 and 1.0. Since $\boldsymbol{R}_s$ remains constant, the SNR is varied by varying the values of σ^2.

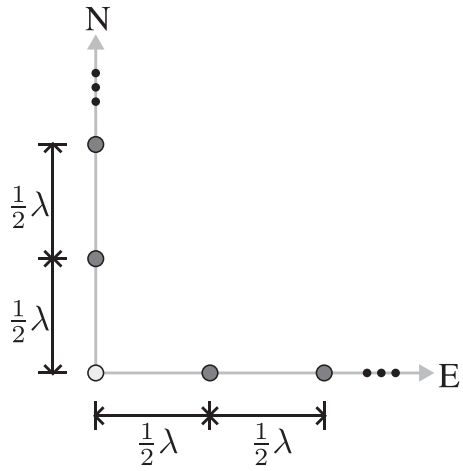

Fig. 3. The L-shaped antenna array as used for the comparison of the SM and DM. The dark grey elements are used for an array with an even number of elements, while the light grey element is added in case of an uneven number of elements.

Although the derived bounds hold for arbitrary antenna array geometries, the experiments presented in this section are based on an L-shaped geometry, as shown in Fig. 3. For an even number of antennas, only the dark grey antennas are used. For an uneven number of antennas the light grey antenna (lower left) is added. The antenna elements are evenly spaced and spatially separated by a distance $d = \lambda/2$. The principal axes are pointing north and east.

As the number of unknowns under the SM are always lower than under the DM, $4 + r$ versus $4 + rn$ respectively, generally speaking we would expect that the SM will outperform the DM. As will be shown in this section, this is the case if the number of sources is relatively high compared to the number of antenna elements. However, if the number of sources is low in comparison to the number of antenna elements, both models perform similar. Also, if the SNR becomes very high, both models performs similar, regardless of the number of sources. Although the number of unknowns is different, the comparison is fair as most unknowns under both models are nuisance parameters and only the three attitude angles are of interest for both situations.

Fig. 4 shows for both the SM and DM the CRBs of the three unknown attitude angels for the situation where $\sigma^2 = 1$ and $m = 25$. Note that the source variance is chosen between 0.75 and 1, hence a noise variance of 1 ($\sigma^2 = 1$) indicates that the noise variance and source variance are equal. Further, the number of sources is varied from 2 up to 24. For a low number of sources, compared to the number of antenna elements, the performance of both signal models is similar. For a large number of sources, however, the SM outperforms the DM significantly.

This behaviour changes if the observation noise σ^2 is changed, which is shown in Fig. 5. In this figure the CRB for the estimation of the attitude angle γ_x is shown. The other attitude angles behave similarly. The CRBs are given as function of σ^2, ranging from 10^{-3} to 10^4 times the source variance ($10^{-3} \leq \sigma^2 \leq 10^4$), and for 5, 15 and 24 sources. As can be seen, for high SNRs (low σ^2), the performance of both models becomes almost identical regardless of the number of sources, suggesting that asymptotically both models perform identical.

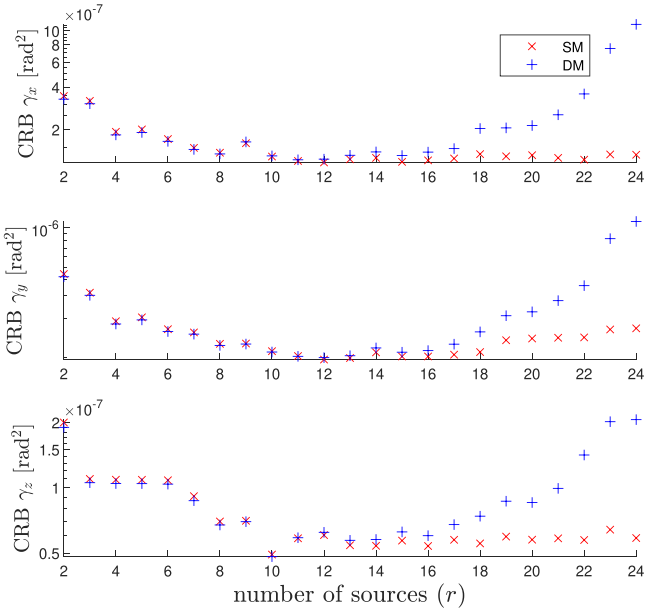

Fig. 4. CRB of γ_x, γ_y and γ_z versus number of sources, with $\sigma^2 = 1$, $m = 25$, $n = 10^3$ and r from 2 up to 24.

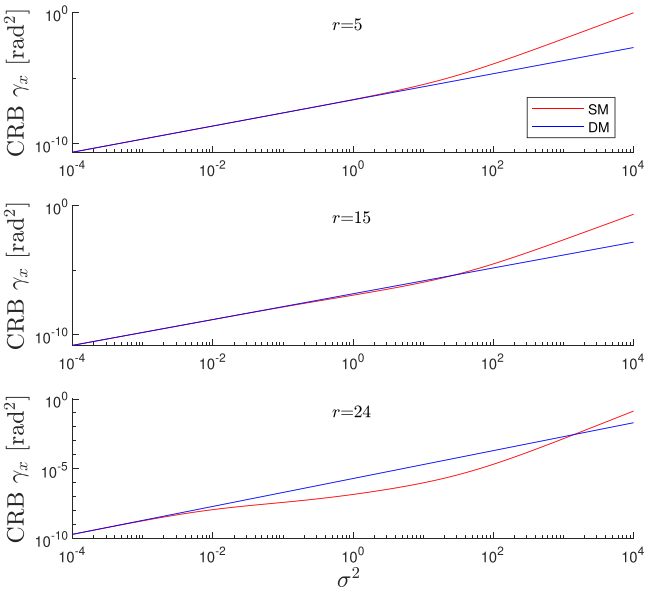

Fig. 5. CRB of γ_x versus σ^2 (different SNR's) for 5, 15 and 24 sources. The number of antenna elements m is 25 and number of samples n is 10^3.

For SNRs where σ^2 is between 10^{-2} and 10^1 time the source variance, the performance is still comparable for a low number of sources compared to the number of antenna elements. However, for a large number of sources, the performance of the SM is superior to that of the DM. This confirms the behaviour shown in Fig. 4 (here $\sigma^2 = 1$), where the performance of both models starts to diverge if the number of sources becomes higher than approximately 15. If the SNR becomes lower, $10^1 \leq \sigma^2 \leq 10^3$, the DM outperforms the SM for a low number of sources. For a large number of sources, the SM still outperforms the DM until σ^2 becomes higher than approximately 10^3 times the

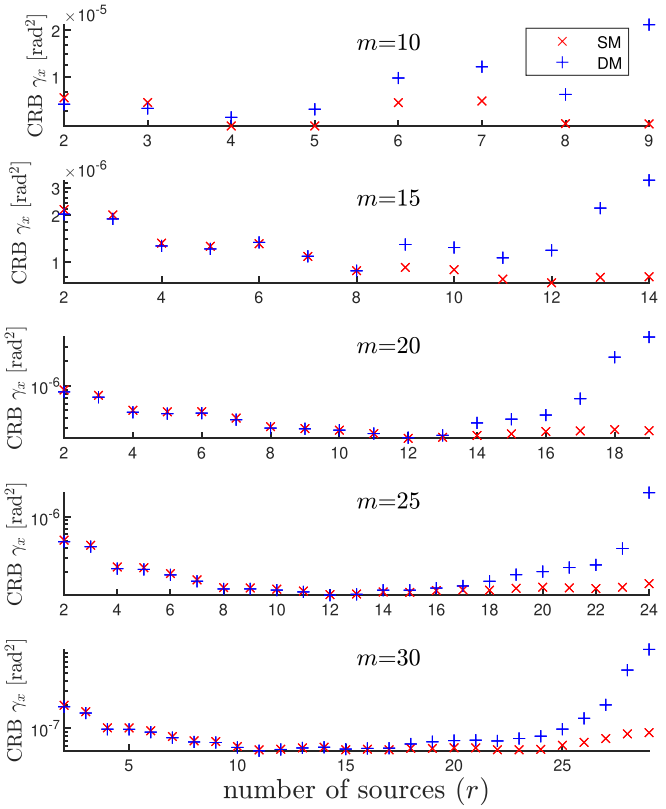

Fig. 6. CRB of γ_x versus the number of sources for different numbers of antenna elements. The number of samples n is 10^3 and σ^2 is equal to 1.

source variance, after which the DM starts to outperform the SM, regardless of the number of sources.

Fig. 6 shows the CRBs for different numbers of antenna elements. The number of elements ranges from 10 to 30 antenna elements. This figure confirms the behaviour of the SM outperforming the DM when the number of sources increases. This behaviour is independent of the number of antenna elements, although it seems that the effect becomes more pronounced with an increasing number of antenna elements. The comparison of the CRBs are based on a fixed source geometry. To show that the provided pictures are indicative for the general behaviour of the bounds, results are recreated based on the median CRB of 100 different randomly chosen source geometries. The results are shown in Fig. 7 where a similar behaviour as the results given in Figs. 4 and 5 is visible, indicating that the used geometry in the analysis is representative. The error bars indicate the first and third quartiles. This figure also shows that for $\sigma^2 > 10^1$ the DM start to outperform the SM for a low number of sources by the red markers (SM), on the left side of the figure, being slightly above the blue markers (DM). This confirms the findings based on Fig. 5. Based on Fig. 5 it is expected that this effect becomes more pronounced for increasing σ^2. In conclusion, we see that the DM and SM perform equally well if the number of sources is about half the number of antenna elements or less, provided that the noise variance is below approximately 10 times the source variance. When the SNR is even higher ($\sigma^2 < 10^{-2}$) the

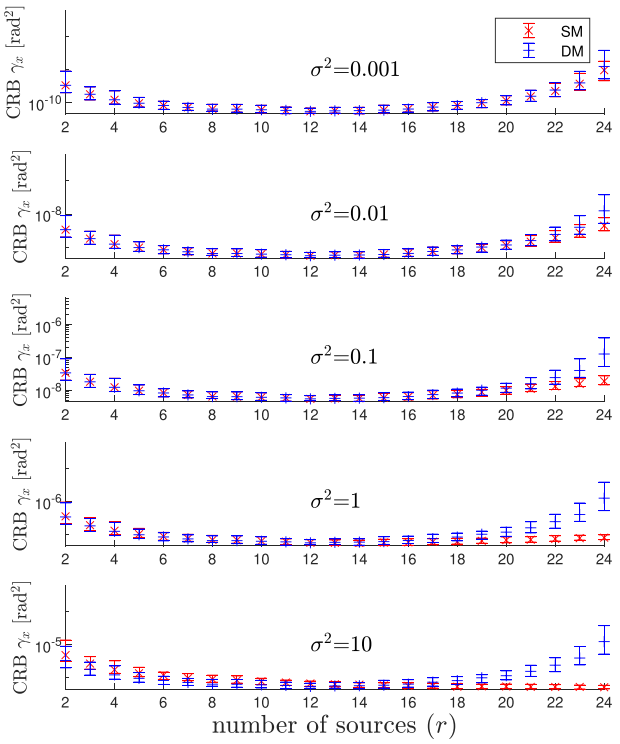

Fig. 7. Median, first and third quartile of the CRB of γ_x versus the number of sources for different values of σ^2. The figure is based on 100 different randomly chosen source geometries. The number of antennas is 25 and the number of samples is 10^3.

performance of both models is equal, regardless of the number of sources.

When the number of sources is relatively high compared to the number of antenna elements, the SM performs better provided that σ^2 is between approximately 10^{-2} and 10^3 times the source variance. If σ^2 increases above 10^3 times the source variance, the DM performs best regardless of the number of antenna elements. So, the choice of the best signal model depends primarily on the SNR and the number of sources relative to the number of antenna elements.

VI. Theoretical Analysis of the CRB

A. Analysis of $\mathrm{CRB}_{\mathrm{DM}}$

To explain the rising CRB if the number of sources approach the number of antenna elements we have to look at (3) or (4). If the number of sources approaches the number of antenna elements, $\boldsymbol{A}(\boldsymbol{A}^H\boldsymbol{A})^{-1}\boldsymbol{A}^H$ becomes close to identity, hence the entries of $\boldsymbol{P}_{\boldsymbol{A}}^{\perp}$ become small and eventually zero when the number of sources equals the number of antenna elements. As the entries of $\boldsymbol{P}_{\boldsymbol{A}}^{\perp}$ get smaller, the entries of the inverse become larger so that $\mathrm{CRB}_{\mathrm{DM}}$ gets larger when the number of sources approaches the number of antenna elements.

On the other hand, if the number of sources is small compared to the number of antenna elements, $\boldsymbol{P}_{\boldsymbol{A}}^{\perp}$ is close to identity. The less sources the closer it gets to identity, so $\partial_{\boldsymbol{\gamma}}(\boldsymbol{A})^H\boldsymbol{P}_{\boldsymbol{A}}^{\perp}\partial_{\boldsymbol{\gamma}}(\boldsymbol{A}) \approx \partial_{\boldsymbol{\gamma}}(\boldsymbol{A})^H\partial_{\boldsymbol{\gamma}}(\boldsymbol{A})$. Further notice that the individual elements of the matrix given by $(\boldsymbol{I}_3 \otimes \mathbf{1}_r)^T\{\partial_{\boldsymbol{\gamma}}(\boldsymbol{A})^H\partial_{\boldsymbol{\gamma}}(\boldsymbol{A})\}(\boldsymbol{I}_3 \otimes \mathbf{1}_r)$ can be written as $\mathrm{tr}(\partial_{\boldsymbol{\gamma}_j}(\boldsymbol{A})^H\partial_{\boldsymbol{\gamma}_l}(\boldsymbol{A}))$ where $j,l \in \{x,y,z\}$. For the diagonal elements of this matrix, for which holds that $j=l$, $\mathrm{tr}(\partial_{\boldsymbol{\gamma}_j}(\boldsymbol{A})^H\partial_{\boldsymbol{\gamma}_j}(\boldsymbol{A}))$ will always increase with an increasing number of sources as the diagonal elements of $\partial_{\boldsymbol{\gamma}_j}(\boldsymbol{A})^H\partial_{\boldsymbol{\gamma}_j}(\boldsymbol{A})$ are always real and positive. So, as the trace increases with the number of sources, the CRB is expected to decrease. We can conclude that for a low number of sources the effect of $\partial_{\boldsymbol{\gamma}}(\boldsymbol{A})^H\partial_{\boldsymbol{\gamma}}(\boldsymbol{A})$ is dominant, while for a large number of sources the effect of $\boldsymbol{P}_{\boldsymbol{A}}^{\perp}$ is dominant. This explains why the bound based on the DM first decreases and later increases with an increasing number of sources.

B. Analysis of $\mathrm{CRB}_{\mathrm{SM}}$

The SM shows the same behaviour as the DM for high SNRs. For low SNRs, however, it is remarkable that the bound does not increase for a large number of sources as the $\mathrm{CRB}_{\mathrm{DM}}$ shows. The elements of the Fisher information matrix for the SM can be determined by (5). Recall that the covariance matrix of the observations is given by

$$\boldsymbol{R} = \boldsymbol{A}\boldsymbol{R}_s\boldsymbol{A}^H + \sigma^2\boldsymbol{I}_m,$$

so that for low SNR we have $\boldsymbol{R} \approx \sigma^2\boldsymbol{I}_m$. With this covariance matrix, (5) can be rewritten as

$$\{\tilde{\boldsymbol{F}}_{\mathrm{SM}}\}_{jl} \approx \frac{n}{\sigma^4}\mathrm{tr}(\partial_{\boldsymbol{\xi}_j}(\boldsymbol{R})\partial_{\boldsymbol{\xi}_l}(\boldsymbol{R})). \tag{7}$$

From this equation we can derive the approximation of the $\mathrm{CRB}_{\mathrm{SM}}$ as given by the Theorem 2.

Theorem 2: The approximation of the $\mathrm{CRB}_{\mathrm{SM}}$ for low SNR is given by

$$\mathrm{CRB}_{\mathrm{SM}} \approx \left(\tilde{\boldsymbol{F}}_{\gamma}\right)^{-1},$$

where

$$\left\{\tilde{\boldsymbol{F}}_{\gamma}\right\}_{ij} = \frac{2n}{\sigma^4}\,\mathrm{Re}\left[\mathrm{tr}\left(\partial_{\gamma_i}(\boldsymbol{A})\boldsymbol{R}_s\boldsymbol{A}^H\partial_{\gamma_j}(\boldsymbol{A})\boldsymbol{R}_s\boldsymbol{A}^H\right) + \mathrm{tr}\left(\partial_{\gamma_i}(\boldsymbol{A})\boldsymbol{R}_s\boldsymbol{A}^H\boldsymbol{A}\boldsymbol{R}_s\partial_{\gamma_j}(\boldsymbol{A})^H\right)\right]. \tag{8}$$

with $i,j \in \{x,y,z\}$.

Proof: See Appendix C. □

Corollary 2: For low SNR and sufficiently large m, the elements of the FIM as given in Theorem 2, can be approximated by

$$\left\{\tilde{\boldsymbol{F}}_{\gamma}\right\}_{ij} \approx \frac{2n\kappa^2 p_k^2}{\sigma^4}\sum_{k=1}^{r}\left\{m\boldsymbol{u}_k^T\partial_{\gamma_i}(\boldsymbol{C})\boldsymbol{G}\boldsymbol{G}^T\partial_{\gamma_j}(\boldsymbol{C})^T\boldsymbol{u}_k - \mathbf{1}_m^T\left[(\boldsymbol{u}_k^T\partial_{\gamma_i}(\boldsymbol{C})\boldsymbol{G}) \otimes (\boldsymbol{u}_k^T\partial_{\gamma_j}(\boldsymbol{C})\boldsymbol{G})^T\right]\mathbf{1}_m\right\} \tag{9}$$

with $i,j \in \{x,y,z\}$.

Proof: Corollary 2 follows from the fact that [25, Fact 7.4.9]

$$\mathrm{tr}(\boldsymbol{A}\boldsymbol{B}\boldsymbol{C}\boldsymbol{D}) = \mathrm{vec}(\boldsymbol{A})^T(\boldsymbol{B} \otimes \boldsymbol{C}^T)\,\mathrm{vec}(\boldsymbol{C}^T)$$

where $\mathrm{vec}(\boldsymbol{A})$ is a vector formed by stacking the columns of $\boldsymbol{A}$, together with the fact that $\boldsymbol{A}^H\boldsymbol{A} \approx m\boldsymbol{I}_r$ and the expression for the steering vectors given by (1). □

For $j=i$ (9) simplifies to

$$\left\{\tilde{\boldsymbol{F}}_{\gamma}\right\}_{ii} \approx \frac{2n\kappa^2 p_k^2}{\sigma^4}\sum_{k=1}^{r}\left\{m\mathbf{1}_m\left(\boldsymbol{u}_k^T\partial_{\gamma_i}(\boldsymbol{C})\boldsymbol{G}\right)^{\circ 2}\right.$$

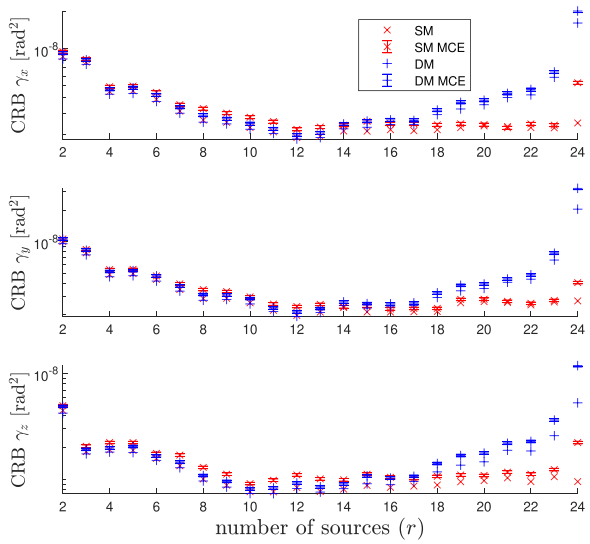

Fig. 8. The results of the MC estimation of the CRB for 2 up to 24 sources, 25 antennas, $\sigma^2 = 1$ and $5 \cdot 10^4$ samples. This MC estimation is based on 10^4 repetitions. The error bars indicate the 95% confidence interval.

$$- \left(\mathbf{1}_m \boldsymbol{u}_k^T \partial_{\gamma_i}(\boldsymbol{C})\boldsymbol{G}\right)^2 \Big\} \tag{10}$$

where $(\cdot)^{\circ 2}$ indicates the element wise square.

Based on the Cauchy–Schwarz inequality, the first element in the summation of (10) is larger than the second element. Hence, each additional signal will increase the elements on diagonal of the FIM and therefore the CRB is expected to decrease, which explains the behaviour of the SM at low SNR.

VII. Validation of CRB

In the previous sections the equations of the CRBs for both the SM and DM are provided, compared and their behaviour analysed. To verify the given expressions, the parameters are estimated using Monte-Carlo (MC) simulations. For this validation the same antenna and source geometry is used as described before.

Observations for $n = 5 \cdot 10^4$ consecutive time samples were generated, resulting in a $25 \times 5 \cdot 10^4$ observation matrix Y. The attitude angles were estimated using maximum likelihood estimation (MLE) which procedure is described in detail in [21]. This is done for both the SM and DM signal models. This was repeated 10^4 times resulting in 10^4 estimated attitude vectors ($\hat{\boldsymbol{\gamma}}$) for both the SM and DM. Next the variance of the estimated attitude was calculated for both models and compared to the CRBs of (4) and (6).

Results of this comparison are presented in Fig. 8. The red $\times$ indicate the CRB for the SM for different numbers of sources and the same symbol including an error bar indicates the Monte-Carlo estimated variance using the SM. The same holds for the DM, where the $+$ symbol is used. The error bars indicate the 95% confidence interval for the estimated variance, based on a variance estimated using 10^4 samples. Fig. 8 shows that the estimated variances of the attitude estimation closely match the calculated CRBs. Only for the situation with 24 sources the estimated variance is much higher than the CRB. The situation with 24 sources and 25 antenna elements is the most challenging situation and therefore the variance estimation is off. To improve the estimation, we need to further increase the number of observations n since the MLE will approach the CRB for $n \to \infty$ [26].

VIII. Conclusion

This contribution compared the performance of the stochastic and deterministic signal models for attitude estimation using signals with unknown structure. For this comparison, the CRBs of the attitude estimation problem are determined for both models. It is shown that for high SNRs, where $\sigma^2 < 10^{-2}$ times the source variance, the performance of both models is equal, regardless of the number of sources. If the SNR decreases, where the noise variance is between 10^{-2} and 10^3 time the source variance, the SM starts to outperform the DM if the number of sources is high compared to the number of antenna elements. For a low number of sources, both models continue to perform equally well until σ^2 is raised to approximately 10^1, where the DM starts to outperform the SM. If σ^2 increases even further ($\sigma^2 > 10^3$), the DM outperforms the SM regardless of the number of sources. The choice of the best signal model, therefore, depends on the SNR and the number of sources relative to the number of antenna elements. Next, the behaviour of the CRBs is theoretically explained based on a simplified two-dimensional situation with a single unknown angle. Finally, the found CRBs are validated using Monte-Carlo simulations where the unknown attitude angles were estimated using maximum likelihood estimators. The results of these Monte-Carlo simulations confirmed the correctness of the CRBs found for both models.

Appendix A
Proof of Theorem 1

Given (2), we have

$$\nabla_{\sigma^2} l(\boldsymbol{\xi}) = -\frac{mn}{\sigma^2} + \frac{1}{\sigma^4}\sum_{t=1}^{n} \|\boldsymbol{y}(t) - \boldsymbol{A}\boldsymbol{s}(t)\|_2^2,$$

$$\nabla_{\boldsymbol{s}^*(t)} l(\boldsymbol{\xi}) = \frac{1}{\sigma^2}\boldsymbol{A}^H(\boldsymbol{y}(t) - \boldsymbol{A}\boldsymbol{s}(t)),\ t = 1, \ldots, n,$$

$$\nabla_{\boldsymbol{s}(t)} l(\boldsymbol{\xi}) = \frac{1}{\sigma^2}\boldsymbol{A}^T(\boldsymbol{y}(t) - \boldsymbol{A}\boldsymbol{s}(t))^*,\ t = 1, \ldots, n.$$

Moreover, the partial derivative with respect to the unknown attitude angle γ_x is given by

$$\frac{\partial}{\partial \gamma_x} l(\boldsymbol{\xi}) = \frac{2}{\sigma^2}\sum_{t=1}^{n} \mathrm{Re}\left\{\boldsymbol{s}^H(t)\partial_{\gamma_x}(\boldsymbol{A})^H(\boldsymbol{y}(t) - \boldsymbol{A}\boldsymbol{s}(t))\right\},$$

and similarly for γ_y and γ_z, which can be compactly expressed as

$$\nabla_{\gamma} l(\boldsymbol{\xi}) = \frac{2}{\sigma^2}\sum_{t=1}^{n} \mathrm{Re}\left\{\boldsymbol{S}_d^H(t)\partial_{\boldsymbol{\gamma}}(\boldsymbol{A})^H(\boldsymbol{y}(t) - \boldsymbol{A}\boldsymbol{s}(t))\right\},$$

where $\boldsymbol{S}_d(t) = \boldsymbol{I}_3 \otimes \boldsymbol{s}(t)$.

Hence, the entries of the FIM associated to σ^2 are given by

$$-\mathbb{E}(\nabla_{\sigma^2}^2 l(\boldsymbol{\xi})) = -\frac{mn}{\sigma^4} + \frac{2}{\sigma^6}\sum_{t=1}^{n} \mathbb{E}(\|\boldsymbol{y}(t) - \boldsymbol{A}\boldsymbol{s}(t)\|^2)$$

$$= -\frac{mn}{\sigma^4} + \frac{2mn\sigma^2}{\sigma^6} = \frac{mn}{\sigma^4},$$

and

$$\mathbb{E}\left(\nabla_{\sigma^2}\nabla^H_{(\cdot)} l(\boldsymbol{\xi})\right) = 0.$$

The FIM entries with respect to the (complex-valued) signals are given by

$$-\mathbb{E}\left(\nabla_{\boldsymbol{s}^*(t)}\nabla^H_{\boldsymbol{s}^*(p)} l(\boldsymbol{\xi})\right) = \frac{1}{\sigma^2}\boldsymbol{A}^H\boldsymbol{A}\delta_{tp},$$

$$-\mathbb{E}\left(\nabla_{\boldsymbol{s}(t)}\nabla^H_{\boldsymbol{s}(p)} l(\boldsymbol{\xi})\right) = \frac{1}{\sigma^2}\boldsymbol{A}^T\boldsymbol{A}^*\delta_{tp},$$

$$-\mathbb{E}\left(\nabla_{\boldsymbol{s}^*(t)}\nabla^H_{\boldsymbol{s}(p)} l(\boldsymbol{\xi})\right) = 0,$$

where δ_{tp} is the Kronecker delta. Finally, the entries with respect to the attitude angles are given by

$$-\mathbb{E}\left(\nabla_{\boldsymbol{\gamma}}\nabla^H_{\boldsymbol{s}^*(t)} l(\boldsymbol{\xi})\right) = \frac{1}{\sigma^2}\boldsymbol{S}_d^H(t)\partial_{\boldsymbol{\gamma}}(\boldsymbol{A})^H\boldsymbol{A},$$

$$-\mathbb{E}\left(\nabla_{\boldsymbol{\gamma}}\nabla^H_{\boldsymbol{s}(t)} l(\boldsymbol{\xi})\right) = \frac{1}{\sigma^2}\boldsymbol{S}_d^T(t)\partial_{\boldsymbol{\gamma}}(\boldsymbol{A})^T\boldsymbol{A}^*,$$

and

$$-\mathbb{E}\big(\nabla_{\boldsymbol{\gamma}}\nabla^H_{\boldsymbol{\gamma}} l(\boldsymbol{\xi})\big) = \frac{2}{\sigma^2}\sum_{t=1}^{n}\mathrm{Re}\big\{\boldsymbol{S}_d^H(t)\partial_{\boldsymbol{\gamma}}(\boldsymbol{A})^H\partial_{\boldsymbol{\gamma}}(\boldsymbol{A})\boldsymbol{S}_d(t)\big\}.$$

With these equations, the FIM for the DM becomes:

$$\boldsymbol{F}_{\mathrm{DM}} = \begin{bmatrix} \boldsymbol{F}_{\sigma^2} & 0 & 0 & 0 \\ 0 & \boldsymbol{F}_{\boldsymbol{s}} & 0 & \boldsymbol{F}_{\boldsymbol{s}^*\boldsymbol{\gamma}} \\ 0 & 0 & \boldsymbol{F}_{\boldsymbol{s}^*} & \boldsymbol{F}_{\boldsymbol{s}\boldsymbol{\gamma}} \\ 0 & \boldsymbol{F}_{\boldsymbol{\gamma}\boldsymbol{s}} & \boldsymbol{F}_{\boldsymbol{\gamma}\boldsymbol{s}^*} & \boldsymbol{F}_{\boldsymbol{\gamma}} \end{bmatrix},$$

where

$$\boldsymbol{F}_{\sigma^2} = \frac{mn}{\sigma^4},$$

$$\boldsymbol{F}_{\boldsymbol{s}^*} = \frac{1}{\sigma^2}\boldsymbol{I}_n \otimes \boldsymbol{A}^H\boldsymbol{A},$$

$$\boldsymbol{F}_{\boldsymbol{s}} = \frac{1}{\sigma^2}\boldsymbol{I}_n \otimes (\boldsymbol{A}^H\boldsymbol{A})^*,$$

$$\boldsymbol{F}_{\boldsymbol{\gamma}\boldsymbol{s}^*} = \frac{1}{\sigma^2}\left[\boldsymbol{S}_d^H(1), \ldots, \boldsymbol{S}_d^H(n)\right]\partial_{\boldsymbol{\gamma}}(\boldsymbol{A})^H\boldsymbol{A},$$

$$\boldsymbol{F}_{\boldsymbol{\gamma}\boldsymbol{s}} = \frac{1}{\sigma^2}\left[\boldsymbol{S}_d^T(1), \ldots, \boldsymbol{S}_d^T(n)\right]\partial_{\boldsymbol{\gamma}}(\boldsymbol{A})^T\boldsymbol{A}^*,$$

$$\boldsymbol{F}_{\boldsymbol{s}^*\boldsymbol{\gamma}} = \boldsymbol{F}^H_{\boldsymbol{\gamma}\boldsymbol{s}^*},$$

$$\boldsymbol{F}_{\boldsymbol{s}\boldsymbol{\gamma}} = \boldsymbol{F}^H_{\boldsymbol{\gamma}\boldsymbol{s}},$$

$$\boldsymbol{F}_{\boldsymbol{\gamma}} = \frac{2}{\sigma^2}\sum_{t=1}^{n}\mathrm{Re}\left\{\boldsymbol{S}_d^H(t)\partial_{\boldsymbol{\gamma}}(\boldsymbol{A})^H\partial_{\boldsymbol{\gamma}}(\boldsymbol{A})\boldsymbol{S}_d(t)\right\}.$$

To find the CRB for the unknown attitude angles we need to calculate the bottom right 3×3 submatrix of $\boldsymbol{F}^{-1}_{\mathrm{DM}}$. This submatrix of the inverse FIM can be found using the standard results on the inverse of partitioned matrices [25, sec. 2.17] as

$$\begin{aligned}
&\mathrm{CRB}_{\mathrm{DM}} \\
&= \left[\boldsymbol{F}_{\boldsymbol{\gamma}} - \left(\boldsymbol{F}_{\boldsymbol{\gamma}\boldsymbol{s}}\boldsymbol{F}_{\boldsymbol{s}}^{-1}\boldsymbol{F}_{\boldsymbol{s}\boldsymbol{\gamma}} + \boldsymbol{F}_{\boldsymbol{\gamma}\boldsymbol{s}^*}\boldsymbol{F}_{\boldsymbol{s}^*}^{-1}\boldsymbol{F}_{\boldsymbol{s}^*\boldsymbol{\gamma}}\right)\right]^{-1} \\
&= \left[\boldsymbol{F}_{\boldsymbol{\gamma}} - 2\,\mathrm{Re}\left(\boldsymbol{F}_{\boldsymbol{\gamma}\boldsymbol{s}^*}\boldsymbol{F}_{\boldsymbol{s}^*}^{-1}\boldsymbol{F}_{\boldsymbol{s}^*\boldsymbol{\gamma}}\right)\right]^{-1} \\
&= \sigma^2\left[2\sum_{t=1}^{n}\mathrm{Re}\left\{\boldsymbol{S}_d^H(t)\partial_{\boldsymbol{\gamma}}(\boldsymbol{A})^H\partial_{\boldsymbol{\gamma}}(\boldsymbol{A})\boldsymbol{S}_d(t)\right.\right. \\
&\quad \left.\left. -\boldsymbol{S}_d^H(t)\partial_{\boldsymbol{\gamma}}(\boldsymbol{A})^H\boldsymbol{A}(\boldsymbol{A}^H\boldsymbol{A})^{-1}\boldsymbol{A}^H\partial_{\boldsymbol{\gamma}}(\boldsymbol{A})\boldsymbol{S}_d(t)\right\}\right]^{-1} \\
&= \sigma^2\left[2\sum_{t=1}^{n}\mathrm{Re}\left\{\boldsymbol{S}_d^H(t)\partial_{\boldsymbol{\gamma}}(\boldsymbol{A})^H\boldsymbol{P}^{\perp}_{\boldsymbol{A}}\partial_{\boldsymbol{\gamma}}(\boldsymbol{A})\boldsymbol{S}_d(t)\right\}\right]^{-1}.
\end{aligned}$$

This completes the proof.

Appendix B
Proof of Corollary 1

Since

$$\frac{1}{n}\sum_{t=1}^{n}\boldsymbol{s}(t)\boldsymbol{s}^H(t) \to \mathbb{E}\left(\boldsymbol{s}(t)\boldsymbol{s}^H(t)\right) = \boldsymbol{R}_s,$$

as $n\to\infty$, we have that

$$\begin{aligned}
&\left(\boldsymbol{S}_d^H(t)\partial_{\boldsymbol{\gamma}}(\boldsymbol{A})^H\boldsymbol{P}^{\perp}_{\boldsymbol{A}}\partial_{\boldsymbol{\gamma}}(\boldsymbol{A})\boldsymbol{S}_d(t)\right)_{jk} \\
&\quad = \boldsymbol{s}^H(t)\partial_{\gamma_j}(\boldsymbol{A})^H\boldsymbol{P}^{\perp}_{\boldsymbol{A}}\partial_{\gamma_k}(\boldsymbol{A})\boldsymbol{s}(t) \\
&\quad = n\mathbf{1}_r^T\left\{\partial_{\gamma_j}(\boldsymbol{A})^H\boldsymbol{P}^{\perp}_{\boldsymbol{A}}\partial_{\gamma_k}(\boldsymbol{A})\odot\boldsymbol{R}_s\right\}\mathbf{1}_r.
\end{aligned}$$

where $j,k\in\{x,y,z\}$ and $(.)_{jk}$ indicates the elements belonging to γ_j and γ_k respectively. Hence

$$\begin{aligned}
&\boldsymbol{S}_d^H(t)\partial_{\boldsymbol{\gamma}}(\boldsymbol{A})^H\boldsymbol{P}^{\perp}_{\boldsymbol{A}}\partial_{\boldsymbol{\gamma}}(\boldsymbol{A})\boldsymbol{S}_d(t) \\
&= n\left(\boldsymbol{I}_3\otimes\mathbf{1}_r\right)^T\left\{\partial_{\boldsymbol{\gamma}}(\boldsymbol{A})^H\boldsymbol{P}^{\perp}_{\boldsymbol{A}}\partial_{\boldsymbol{\gamma}}(\boldsymbol{A})\odot(\mathbb{1}_3\otimes\boldsymbol{R}_s)\right\} \\
&\quad (\boldsymbol{I}_3\otimes\mathbf{1}_r),
\end{aligned}$$

so that $\mathrm{CRB}_{\mathrm{DM}} = \sigma^2[2n\,\mathrm{Re}\{(\boldsymbol{I}_3\otimes\mathbf{1}_r)^T\{\partial_{\boldsymbol{\gamma}}(\boldsymbol{A})^H\boldsymbol{P}^{\perp}_{\boldsymbol{A}}\partial_{\boldsymbol{\gamma}}(\boldsymbol{A}) \odot(\mathbb{1}_3\otimes\boldsymbol{R}_s)\}(\boldsymbol{I}_3\otimes\mathbf{1}_r)\}]^{-1}$. This completes the proof.

Appendix C
Proof of Theorem 2

Given (7), we need to find the derivatives of R with respect to the unknown parameters. These derivatives are given by

$$\partial_{\gamma_x}(\boldsymbol{R}) = \partial_{\gamma_x}(\boldsymbol{A})\boldsymbol{R}_s\boldsymbol{A}^H + \boldsymbol{A}\boldsymbol{R}_s\partial_{\gamma_x}(\boldsymbol{A})^H,$$

and similarly for $\partial_{\gamma_y}(\boldsymbol{R})$ and $\partial_{\gamma_z}(\boldsymbol{R})$,

$$\partial_{\sigma^2}(\boldsymbol{R}) = \boldsymbol{I}_m,$$

$$\partial_{p_i}(\boldsymbol{R}) = \boldsymbol{a}_i\boldsymbol{a}_i^H.$$

Now the elements of the FIM, which is given by

$$\tilde{\boldsymbol{F}}_{\mathrm{SM}} = \begin{bmatrix} \tilde{\boldsymbol{F}}_{\sigma^2} & \tilde{\boldsymbol{F}}_{\sigma^2 p} & \tilde{\boldsymbol{F}}_{\sigma^2\boldsymbol{\gamma}} \\ \tilde{\boldsymbol{F}}_{p\sigma^2} & \tilde{\boldsymbol{F}}_{p} & \tilde{\boldsymbol{F}}_{p\boldsymbol{\gamma}} \\ \tilde{\boldsymbol{F}}_{\boldsymbol{\gamma}\sigma^2} & \tilde{\boldsymbol{F}}_{\boldsymbol{\gamma}p} & \tilde{\boldsymbol{F}}_{\boldsymbol{\gamma}} \end{bmatrix},$$

can be determined. The element with respect to σ^2 is given by

$$\tilde{\boldsymbol{F}}_{\sigma^2} = \frac{nm}{\sigma^4}.$$

For sufficiently large m the elements with respect to p become

$$\{\tilde{\boldsymbol{F}}_p\}_{ij} = \frac{n}{\sigma^4}\mathrm{tr}\left(\boldsymbol{a}_i\boldsymbol{a}_i^H\boldsymbol{a}_j\boldsymbol{a}_j^H\right),$$

$$i,j = 1,\ldots,r = \frac{n}{\sigma^4}\boldsymbol{a}_j^H\boldsymbol{a}_i\boldsymbol{a}_i^H\boldsymbol{a}_j, \approx \frac{nm^2}{\sigma^4}\delta_{ij},$$

thus, the total submatrix of the FIM with respect to p becomes

$$\tilde{\boldsymbol{F}}_p = \frac{nm^2}{\sigma^4}I_r.$$

For the elements with respect to $\boldsymbol{\gamma}$ we find

$$\begin{aligned}\left\{\tilde{\boldsymbol{F}}_\gamma\right\}_{ij} &= \frac{n}{\sigma^4}\mathrm{tr}\left[\left(\partial_{\gamma_i}(\boldsymbol{A})\boldsymbol{R}_s\boldsymbol{A}^H + \boldsymbol{A}\boldsymbol{R}_s\partial_{\gamma_i}(\boldsymbol{A})^H\right)\right.\\ &\left.\left(\partial_{\gamma_j}(\boldsymbol{A})\boldsymbol{R}_s\boldsymbol{A}^H + \boldsymbol{A}\boldsymbol{R}_s\partial_{\gamma_j}(\boldsymbol{A})^H\right)\right], \quad i,j = \{x,y,z\}\\ &= \frac{2n}{\sigma^4}\mathrm{Re}\left[\mathrm{tr}\left(\partial_{\gamma_i}(\boldsymbol{A})\boldsymbol{R}_s\boldsymbol{A}^H\partial_{\gamma_j}(\boldsymbol{A})\boldsymbol{R}_s\boldsymbol{A}^H\right)\right.\\ &\left.+\mathrm{tr}\left(\partial_{\gamma_i}(\boldsymbol{A})\boldsymbol{R}_s\boldsymbol{A}^H\boldsymbol{A}\boldsymbol{R}_s\partial_{\gamma_j}(\boldsymbol{A})^H\right)\right]. \qquad (11)\end{aligned}$$

For the cross terms between σ^2 and p we find

$$\tilde{\boldsymbol{F}}_{\sigma^2 p_i} = \frac{n}{\sigma^4}\mathrm{tr}(\boldsymbol{a}_i\boldsymbol{a}_i^H), = \frac{n}{\sigma^4}\boldsymbol{a}_i^H\boldsymbol{a}_i, = \frac{nm}{\sigma^4}.$$

And for the other cross terms between γ, p and σ^2 we find respectively

$$\begin{aligned}\tilde{\boldsymbol{F}}_{\gamma_j p_i} &= \frac{n}{\sigma^4}\mathrm{tr}\left[\left(\partial_{\boldsymbol{\gamma}_j}(\boldsymbol{A})\boldsymbol{R}_s\boldsymbol{A}^H + \boldsymbol{A}\boldsymbol{R}_s\partial_{\boldsymbol{\gamma}_j}(\boldsymbol{A})^H\right)\boldsymbol{a}_i\boldsymbol{a}_i^H\right]\\ &= \frac{2n}{\sigma^4}\mathrm{tr}\left[\mathrm{Re}\left(\boldsymbol{a}_i^H\partial_{\boldsymbol{\gamma}_j}(\boldsymbol{A})\boldsymbol{R}_s\boldsymbol{A}^H\boldsymbol{a}_i\right)\right]\\ &\approx \frac{2nmp_i}{\sigma^4}\mathrm{Re}\left(\boldsymbol{a}_i^H\partial_{\boldsymbol{\gamma}_j}(\boldsymbol{a}_i)\right) = 0\end{aligned}$$

and

$$\tilde{\boldsymbol{F}}_{\gamma_j\sigma^2} = \frac{n}{\sigma^4}\mathrm{tr}\left(\partial_{\boldsymbol{\gamma}_j}(\boldsymbol{A})\boldsymbol{R}_s\boldsymbol{A}^H + \boldsymbol{A}\boldsymbol{R}_s\partial_{\boldsymbol{\gamma}_j}(\boldsymbol{A})^H\right), = 0,$$

where $j \in \{x,y,z\}$. With these elements of the FIM, we conclude that

$$\tilde{\boldsymbol{F}}_{\mathrm{SM}} = \begin{bmatrix}\tilde{\boldsymbol{F}}_{\sigma^2} & \tilde{\boldsymbol{F}}_{\sigma^2 p} & 0\\ \tilde{\boldsymbol{F}}_{p\sigma^2} & \tilde{\boldsymbol{F}}_p & 0\\ 0 & 0 & \tilde{\boldsymbol{F}}_{\boldsymbol{\gamma}}\end{bmatrix},$$

If we are only interested in the minimum variance of the attitude angles $\boldsymbol{\gamma}$, the CRB is given by

$$\mathrm{CRB}_{\mathrm{SM}} \approx (\tilde{\boldsymbol{F}}_\gamma)^{-1}.$$

where the elements of $\tilde{\boldsymbol{F}}_\gamma$ are given by (11). This completes the proof.

REFERENCES

[1] P. Gupta and S. Kar, "MUSIC and improved MUSIC algorithm to estimate direction of arrival," in *Proc. Int. Conf. Commun. Signal Process.*, 2015, pp. 0757–0761.

[2] X. Zhang and R. Cao, "Direction of arrival estimation: Introduction," in *Wiley Encyclopedia of Electrical and Electronics Engineering*. Hoboken, NJ, USA: Wiley, 2017, pp. 1–22.

[3] M. D. Markel, "Interference mitigation for GPS based attitude determination," Ph.D. dissertation, Graduate Fac. College Eng. Graduate School, Univ. Florida, Gainesville, FL, USA, 2002.

[4] M. Markel, E. Sutton, and H. Zmuda, "An antenna array-based approach to attitude determination in a jammed environment," in *Proc. 14th Int. Tech. Meeting Satell. Division Inst. Navigation*, 2001, pp. 2914–2926.

[5] M. Markel, E. Sutton, and H. Zinuda, "Optimal anti-jam attitude determination using the global positioning system," in *Proc. IEEE Position Location Navigation Symp.*, 2002, pp. 12–19.

[6] P. D. Groves, *Principles of GNSS, Inertial, and Multisensor Integrated Navigation Systems* (GNSS/GPS Series), 2nd ed. Artech House, Boston, London, 2013.

[7] C. E. Cohen, *Attitude Determination Using GPS: Development of an All Solid State Guidance, Navigation, and Control Sensor for Air and Space Vehicles Based on the Global Positioning System*. Ph.D. dissertation, Stanford, CA, USA: Stanford Univ., 1993.

[8] P. J. Buist, "The baseline constrained LAMBDA method for single epoch, single frequency attitude determination applications," in *Proc. 20th Int. Tech. Meeting Satell. Division Inst. Navigation*, 2007, vol. 3, pp. 2962–2973.

[9] A. Raskaliyev, S. Patel, T. Sobh, and A. Ibrayev, "GNSS-Based attitude determination techniques—A comprehensive literature survey," *IEEE Access*, vol. 8, pp. 24873–24886, Jan. 2020.

[10] P. J. G. Teunissen, "Least squares estimation of the integer GPS ambiguities," in *Proc. Invited Lecture, Sect. IV Theory Methodol., IAG Gen. Meeting*, Beijing, China, 1993, pp. 1–16.

[11] S. Verhagen, "The GNSS integer ambiguities: Estimation and validation," Ph.D. dissertation, Delft Ins. Earth Observ. Space Syst., Delft Univ. Technol., Delft, The Netherlands, 2005.

[12] G. Giorgi, "GNSS carrier phase-based attitude determination, estimation and applications," Ph.D. dissertation, Delft Ins. Earth Observ. Space Syst., Delft Univ. Technol., Delft, The Netherlands, 2011.

[13] P. J. Buist, "Multi-platform integrated positioning and attitude determination using GNSS," Ph.D. dissertation, Delft Ins. Earth Observ. Space Syst., Delft Univ. Technol., Delft, Netherlands, 2013.

[14] M. Meurer, A. Konovaltsev, M. Cuntz, and C. Hättich, "Robust joint multi-antenna spoofing detection and attitude estimation using direction assisted multiple hypotheses RAIM," in *Proc. 25th Int. Tech. Meeting Satell. Division Inst. Navigation*, 2012, pp. 3007–3016.

[15] S. Daneshmand, N. Asl, and G. Lachapelle, "Precise GNSS attitude determination based on antenna array processing," in *Proc. 27th Int. Tech. Meeting Satell. Division Inst. Navigation*, 2014, vol. 3, pp. 2555–2562.

[16] B. Parkinson and J. Spilker, *Global Positioning System: Theory and Applications, Volume II* (Progress in Astronautics and Aeronautics Series). Washington, DC, USA: American Institute Aeronautics Astronautics, Inc., 1996.

[17] F. S. Prol et al., "Position, navigation, and timing (PNT) through low earth orbit (LEO) satellites: A survey on current status, challenges, and opportunities," *IEEE Access*, vol. 10, pp. 83971–84002, 2022.

[18] G. Curzi, D. Modenini, and P. Tortora, "Large constellations of small satellites: A survey of near future challenges and missions," *Aerospace*, vol. 7, no. 9, 2020, Art. no. 133.

[19] G. W. Hein, "Status, perspectives and trends of satellite navigation," *Satell. Navigation*, vol. 1, no. 1, 2020, Art. no. 22.

[20] P. Bernhard, M. Deschamps, and G. Zaccour, "Large satellite constellations and space debris: Exploratory analysis of strategic management of the space commons," *Eur. J. Oper. Res.*, vol. 304, no. 3, pp. 1140–1157, 2023.

[21] B. Ottersten, M. Viberg, P. Stoica, and A. Nehorai, "Exact and large sample maximum likelihood techniques for parameter estimation and detection in array processing," in *Radar Array Processing*, S. Haykin, J. Litva, and T. J. Shepherd, Eds. Berlin, Germany: Springer, 1993, pp. 99–151.

[22] P. Stoica and A. Nehorai, "Performance study of conditional and unconditional direction-of-arrival estimation," *IEEE Trans. Acoust., Speech, Signal Process.*, vol. 38, no. 10, pp. 1783–1795, Oct. 1990.

[23] H. Van Trees, K. Bell, and Z. Tian, *Detection Estimation and Modulation Theory, Part I: Detection, Estimation, and Filtering Theory* (Detection Estimation and Modulation Theory Series). Hoboken, NJ, USA: Wiley, 2013.

[24] D. H. Brandwood, "A complex gradient operator and its application in adaptive array theory," *IEE Proc. H Microw. Opt. Antennas*, vol. 130, pp. 11–16, Feb. 1983.

[25] D. S. Bernstein, *Matrix Mathematics: Theory, Facts, and Formulas*, vol. 2, 2nd ed. Princeton, NJ, USA: Princeton Univ. Press, 2009.

[26] S. M. Kay, *Fundamentals of Statistical Signal Processing: Estimation Theory*. Hoboken, NJ, USA: Prentice-Hall, Inc., 1993.